Combined Quantum Chemistry and Photoelectron Spectroscopy Study of the Electronic Structure and Reduction Potentials of Rubredoxin Redox Site Analogues

Shuqiang Niu,[†] Xue-Bin Wang,[‡,§] Jeffrey A. Nichols,[§] Lai-Sheng Wang,*[,‡,§] and Toshiko Ichiye*[,†]

School of Molecular Biosciences, Washington State University, Pullman, Washington 99164-4660, Department of Physics, Washington State University, 2710 University Drive, Richland, Washington 99352, and W. R. Wiley Environmental Molecular Science Laboratory, Pacific Northwest National Laboratory, P.O. Box 999, Richland, Washington 99352

Received: February 6, 2003

Iron−sulfur proteins are an important class of electron carriers in a wide variety of biological reactions. Determining the intrinsic contribution of the metal site to the redox potential is crucial in understanding how the protein environment influences the overall redox properties of the Fe−S proteins. Here we combine density functional theory and coupled cluster methods with photodetachment spectroscopy to study the electronic structures and gas-phase redox potentials of the $[Fe(SCH_3)_4]^{2-/-/0}$ and $[Fe(SCH_3)_3]^{-/0}$ analogues of the rubredoxin redox site. The calculations show that oxidations of $[Fe(SCH_3)_4]^{2-}$ and $[Fe(SCH_3)_4]^{-}$ involve mainly the Fe 3d and S 3p orbitals, respectively. The calculated adiabatic and vertical detachment energies are in good agreement with the experiment for $[Fe(SCH_3)_3]^{-}$ and $[Fe(SCH_3)_4]^{-}$. The current results further confirm the "inverted level scheme" for the high-spin [1Fe] systems. The redox couple, $[Fe(SCH_3)_4]^{-/2-}$, which is the one found in rubredoxin, but cannot be accessed experimentally in the gas phase, was investigated using a thermodynamic cycle that relates it to the $[Fe(SCH_3)_3]^{-/0}$ couple and the ligand association reaction, $[Fe(SCH_3)_3]^{0/-} + SCH_3^- \rightarrow [Fe(SCH_3)_4]^{-/2-}$. The calculated reduction energy of $[Fe(SCH_3)_4]^{-}$ (1.7 eV) compares well with the value (1.6 eV) estimated from the calculated bond energies and the experimental detachment energy of $[Fe(SCH_3)_3]^{-}$. Thus, this thermodynamic cycle method can be used to estimate metal−ligand bonding energies and determine intrinsic reduction potentials from photodetachment experiments when the reduced forms are not stable in the gas phase.

Introduction

In biological systems, electron-transfer proteins serve key roles as electron carriers in a wide variety of processes such as photosynthesis, respiration, nitrogen fixation, and hydrogen metabolism.[1−7] Iron−sulfur proteins are ubiquitous in living systems[8] and they constitute an important class of electron-transfer proteins. They have also been found to play a critical role in enzymatic processes, regulation of gene expression, generation of radicals, and delivery of sulfur and iron for the synthesis of other biomolecules. Generally, the redox sites of Fe−S proteins consist of one to four irons tetrahedrally coordinated by cysteine residues and inorganic sulfurs. Many inorganic analogues of these redox sites have been synthesized and characterized.[9] The simplest of the biological Fe−S redox sites is $[Fe(SR)_4]^{-/2-}$, which contains only a single Fe with four tetrahedral sulfur ligands from cysteine residues. The inorganic core is sometimes referred to as a [1Fe] cluster. This simple redox site is found in relatively small proteins, such as rubredoxin (Rd),[10a] desulforedoxin,[10b] desulfoferrodoxin, rubrerythrin, and nigerythrin.[10c,d] Available experimental evidence suggests that the function of these proteins is as electron-transfer agents in cells,[11] as well as possible roles in superoxide reduction.[12]

The reduction potential of an electron-transfer protein is one of its most important functional characteristics.[8−14] Theoretically, the standard reduction potential (E^0) can be related to the free energy of the reduction reaction (ΔG^0) by the Nernst equation:

$$\Delta G^0 - \Delta\mathrm{NHE} = -nFE^0 \quad (1)$$

where n is the number of electrons transferred, F (=23.06 kcal/(mol·V)) is the Faraday's constant, and ΔNHE is $-4.43F$ V, a known constant energy to reference the "absolute" free energy to the normal hydrogen electrode (NHE).[15] ΔG^0 can be divided into the intrinsic reduction free energy (ΔG_{int}) of the redox site independent of the protein, the extrinsic free energy (ΔG_{env}) due to the protein surrounding and solvent at the redox site, and the perturbative interaction between the two ($\Delta G_{\mathrm{int/env}}$):[3]

$$\Delta G^0 = \Delta G_{\mathrm{int}} + \Delta G_{\mathrm{env}} + \Delta G_{\mathrm{int/env}} \quad (2)$$

Moreover, the intrinsic reduction energy, ΔE_{int}, is approximately equal to the gas-phase reduction energy of a redox site analogue, i.e., the electron detachment energy obtained by photodetachment photoelectron spectroscopy (PES), as schematically shown in Figure 1.[16] Hence,

$$\Delta E_{\mathrm{int}} \sim -\mathrm{ADE} = -(\mathrm{VDE} + \lambda_{\mathrm{oxd}}) \quad (3)$$

where ADE and VDE are the adiabatic and vertical detachment energies, respectively, and λ_{oxd} is the oxidant intramolecular relaxation or reorganization energy.

[†] School of Molecular Biosciences, Washington State University.
[‡] Department of Physics, Washington State University.
[§] Pacific Northwest National Laboratory.

10.1021/jp034316f CCC: $25.00
Published on Web 04/01/2003

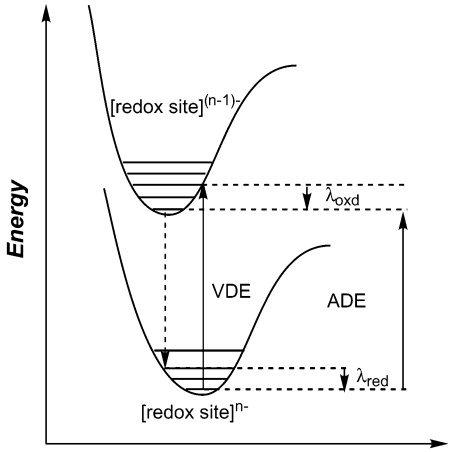

Figure 1. Schematic potential curves showing photodetachment of a $[\text{redox site}]^{n-}$ to a $[\text{redox site}]^{(n-1)-}$. VDE and ADE are the vertical and adiabatic potential energies, respectively. λ_{oxd} and λ_{red} are the intramolecular relaxation energies of $[\text{redox site}]^{n-}$ and $[\text{redox site}]^{(n-1)-}$, respectively (see ref 16).

Understanding how the intrinsic and extrinsic factors contribute to the reduction potential is essential in engineering proteins with different redox properties. The reduction potentials of the $[Fe(SCys)_4]^{-/2-}$ couple among various Rds range from about −95 to +60 mV vs NHE.[8a] This range has been attributed to extrinsic factors, including modulation by the positioning and orientation of peptide dipoles around the metal center.[13a,17] In addition, the reduction potential in rubrerythrin is ∼200 mV, which is higher than in rubredoxin, most likely due to addition of more polar groups.[18] The reduction potentials of synthetic $[Fe(SR)_4]^{-/2-}$ complexes in various solvents range from −114 to −832 mV vs NHE,[19b,c] which is also attributed mainly to extrinsic effects due to the different solvents.[19a,20] However, the separation into intrinsic and extrinsic contributions to reduction potentials is not exact due to perturbative interactions of the redox site with the environment.[21] For example, the redox site may affect the electronic and structural properties of the nearby protein and solvent, and vice versa. This perturbative effect is generally presumed to be small for Fe−S proteins, but it has not been well tested. Thus, characterizing both the intrinsic reduction potential of the redox site and the extrinsic electric field arising from the surrounding protein and solvent at the redox site is important in understanding the molecular determinants of the reduction potentials of Fe−S proteins. In particular, a detailed knowledge of how intrinsic factors affect the reduction potential requires studies of simple $[Fe(SR)_4]^{-/2-}$ complexes in the gas phase, where there is no extrinsic contribution.

A variety of experimental studies have provided information on the electronic structure of the [1Fe] cluster. The electronic structure and bonding of $FeCl_4^-$, $Fe(o\text{-}C_6H_4(CH_2S)_2)_2^-$, $Fe(o\text{-}C_6H_4(CH_2S)_2)_2^{2-}$, and Rds were studied previously by PES and ligand K-edge X-ray absorption spectroscopy.[22] The valence-band spectral similarities of both model complexes and Rds indicate that their electronic structures are identical. The experimental data and Xα calculations confirm the "inverted level scheme" in these systems, where the Fe 3d α levels are found to lie below the ligand-based levels in energy. Our recent development of a PES apparatus coupled with an electrospray ion source allows the electronic structures of multiply charged anions to be examined for the first time in the gas phase[23] and provides an excellent opportunity to obtain the reduction potentials of solution-phase inorganic metal complexes in the gas phase.[16,24] More recently, we investigated the electronic structure and electron detachment (oxidation) energies of several gaseous Rd analogues, $[Fe(SCH_3)_4]^-$ and $[Fe(S_2\text{-}o\text{-}xyl)_2]^-$ as well as $FeCl_4^-$ and $[Fe(SCN)_4]^-$, which all contain an Fe^{III}.[16,25] The corresponding Fe^{II} complexes were not stable gaseous dianions, but the three ligand analogues, $FeCl_3^-$, $[Fe(SCN)_3]^-$, and $[Fe(SCH_3)_3]^-$, and the ion-pair $Na^+[Fe(S_2\text{-}o\text{-}xyl)_2]^{2-}$, which all contain an Fe^{II}, were studied. It was shown that detachment in all the Fe^{II} complexes involves an Fe 3d electron, whereas that of the Fe^{III} complexes may involve primarily ligand-based orbitals.[16,25] However, the redox couple $[Fe(SR)_4]^{-/2-}$ found in rubredoxin and rubrerythrin could not be examined directly by PES because the reduced species is not stable in the gas phase.

Computational chemistry has also been valuable in understanding reduction potentials of [1Fe] clusters both in analogues and in proteins. The electronic structures and reduction potentials of Fe−S clusters have been extensively investigated using a broken symmetry density functional theory (DFT) method.[26] The calculated reduction potentials are comparable to experimental values, even though a continuum dielectric model for the solvent and constrained geometries were used. In addition, we have investigated the electronic properties and conformational dependence of an analogue of the Rd redox site using conventional ab initio methods,[27a−c] and the environmental contribution in Rd by molecular mechanics studies.[17,20] Results include the successful prediction of the Ala-Val sequence determinant at residue 44,[17a] the effects of other mutants at residue 44,[17b] and penetration of water through nonpolar side chain "water gates",[20b,c] which have all been verified experimentally.[13] The effects of metal substitution in the $[M(SR)_4]^{2-/-}$ analogues have also been examined for M = Fe, Co, Ni, and Zn.[27b] Furthermore, recent progress in combined quantum mechanical/molecular mechanical (QM/MM) methods provides the possibility of investigating and understanding environmental effects on the electronic properties of Fe−S proteins.[28] For instance, the geometries and reorganization energies of Rd and [2Fe−2S] ferredoxin have been studied using a QM/MM method.[28b]

Advances in DFT methods have prompted new investigations of the electronic structures and redox properties of Fe−S active sites. Hybrid generalized gradient approximation (GGA) methods,[29] which have some exact Hartree−Fock (HF) exchange included, have become a major computational tool for treating transition-metal systems because these methods appear to be more efficient and accurate, especially for the first-row transition-metal systems.[30] In a recent study,[27d] we calculated $[Fe(SCH_3)_4]^{2-/-/0}$ and $[Fe(SCH_3)_3]^{-/0}$ at different levels of theory and with different basis sets to determine the best optimization and energy correlation methods. For geometry optimization, the hybrid GGA methods tested were the Becke three parameter hybrid exchange functional[31] with the Lee−Yang−Parr (B3LYP),[32] Becke's "*half and half*" functionals (BHandH),[33c] and a modified Becke's 10-parameter functional (B97gga1),[29b] with both full basis sets and effective core potential (ECP) basis sets. For energetics, B3LYP, B97gga1, the Møller−Plesset perturbation series (MP2, MP3, MP4SDQ), and coupled cluster singles and doubles (CCSD)[29] as well as CCSD with perturbative corrections for triples [CCSD(T)] methods were tested using both full and ECP basis sets. The major conclusions were (i) the 6-31G** basis sets alone or with added diffuse or polarization functions on the sulfurs at the B3LYP level gave the best overall description of the geometry, in which the Fe−S and S−C bond lengths were only slightly longer (<0.06 Å) than experimental values and the increase in Fe−S bond length upon reduction was only slightly (∼0.01 Å) more than the experimental value and (ii) adding diffuse functions to the basis

TABLE 1: Experimental and B3LYP/6-31G Optimized Fe−S (r_{Fe-S}) Bond Lengths (Å) and ∠S−Fe−S (θ_{S-Fe-S}) Bond Angles (deg) for $[Fe(SCH_3)_4]^{2-}$, $[Fe(SCH_3)_4]^{-}$, $[Fe(SCH_3)_4]^{0}$, $[Fe(SCH_3)_3]^{-}$, and $[Fe(SCH_3)_3]^{0}$**

		r_{Fe-S}		θ_{S-Fe-S}[a]		θ_{S-Fe-S}[b]	
species	S	calc	exp	calc	exp	calc	exp
$[Fe(SCH_3)_4]^{2-}$	2	2.414 ± 0.000	2.356 ± 0.000[c]	110.5 ± 0.0	109.5 ± 6.0	109.0 ± 1.6	109.5 ± 6.0
$[Fe(SCH_3)_4]^{-}$	$^5/_2$	2.314 ± 0.000	2.267 ± 0.000[c]	110.7 ± 0.0	109.5 ± 3.7	108.8 ± 1.9	109.5 ± 3.7
$[Fe(SCH_3)_4]^{0}$	2	2.224 ± 0.006	NA	127.4 ± 0.4	NA	101.3 ± 5.3	NA
$[Fe(SCH_3)_4]^{0}$	1	2.147 ± 0.001	2.185 ± 0.000[d]	117.0 ± 0.1	NA	106.2 ± 10.6	NA
$[Fe(SCH_3)_4]^{0}$	0	2.119 ± 0.000	NA	114.3 ± 0.1	NA	107.3 ± 7.0	NA
$[Fe(SCH_3)_3]^{-}$	2	2.309 ± 0.001	2.274 ± 0.011[e]	120.4 ± 0.2	121.7 ± 0.3	119.3 ± 0.0	116.0 ± 0.0
$[Fe(SCH_3)_3]^{0}$	$^5/_2$	2.209 ± 0.000	NA	120.0 ± 0.0	NA	120.0 ± 0.0	NA

[a] For $[Fe(SCH_3)_4]^n$, θ_{S-Fe-S} refers to average of $\angle S_1-Fe-S_4$ and $\angle S_2-Fe-S_3$. For $[Fe(SCH_3)_3]^n$, θ_{S-Fe-S} refers to average of $\angle S_1-Fe-S_2$ and $\angle S_2-Fe-S_3$. [b] For $[Fe(SCH_3)_4]^n$, θ_{S-Fe-S} refers to average of $\angle S_1-Fe-S_2$, $\angle S_1-Fe-S_3$, $\angle S_3-Fe-S_4$, and $\angle S_2-Fe-S_4$. For $[Fe(SCH_3)_3]^n$, θ_{S-Fe-S} refers to $\angle S_1-Fe-S_3$. [c] $[Fe(S_2\text{-o-xyl})_2]^{2-/-}$, ref 34b. [d] $[Fe(\text{“}S_2\text{”})_2(PMe_3)]^0$, ref 34c. [e] $[Fe(SC_6H_2\text{-}2,4,6\text{-}t\text{-}Bu_3)_3]^{1-}$, ref 34a.

sets at the B3LYP level significantly improved the accuracy of the calculated oxidation potentials of the $[Fe(SCH_3)_3]^{-/0}$ and $[Fe(SCH_3)_4]^{-/0}$ redox couples.

Here, we present a study of the reduction potential of $[Fe(SCH_3)_4]^{-/2-}$, which is the same redox couple as the rubredoxins. This analogue has proved to be a necessary and sufficient model to obtain geometries similar to the active site of the protein.[27b] The computational results are compared with the experimental electronic structure data from gas-phase PES.[16] Because the detachment energy of $[Fe(SCH_3)_4]^{2-}$ cannot be directly measured by PES,[16] here a thermodynamic cycle is devised to estimate this energy from the redox couples, $[Fe(SCH_3)_4]^{-/0}$ and $[Fe(SCH_3)_3]^{-/0}$. Studies of these analogues allow the geometry, electronic structure, and intrinsic reduction potential of the [1Fe] redox site analogue to be understood to a degree of accuracy not possible for the redox site in a protein or for Fe−S sites with more irons. Moreover, the calculation of the electronic structures and oxidation potentials of $[Fe(SCH_3)_4]^{-/0}$ and $[Fe(SCH_3)_3]^{-/0}$ may provide reliable information to characterize the experimental detachment features, redox properties, and iron−sulfur cluster assembly mechanisms of biological molecules.

Computational Details

B3LYP calculations were performed for the tetraligand $[Fe(SCH_3)_4]^{2-/-/0}$ and triligand $[Fe(SCH_3)_3]^{-/0}$ complexes. A “D_{2d}” ML_4 structure, similar to the geometry of the Rd redox site and the lowest energy conformation of a previous study,[27a] is utilized here as the initial theoretical model for $[Fe(SCH_3)_4]^{2-/-/0}$ although no symmetry restraints were imposed during geometry optimizations. A “C_{3h}” ML_3 structure, similar to the geometry of the $[Fe(SC_6H_2\text{-}2,4,6\text{-}t\text{-}Bu_3)_3]^-$ complex[34a] and the lowest energy conformation at the B3LYP/6-31G** level,[27d] is used as the initial $[Fe(SCH_3)_3]^{-/0}$ model.

Two different basis sets are implemented for the geometry optimization and energy correlation at different levels of theory. The first one, referred to here as 6-31G**, is the standard 6-31G basis sets with f-type polarization functions for the iron atom,[35a] d-type polarization functions for the carbon and sulfur atoms, and p-type polarization function for the hydrogen atoms.[35b,c] The second basis sets, referred to here as 6-31(++)$_S$G**, are similar to 6-31G**, but sp-type diffuse functions (6-31++G**) are added to the sulfur atoms.[36]

The calculated VDE and ADE are also refined at different levels of theory with different basis sets. The notation *Method(E)/Basis(E)//Method(G)/Basis(G)* will be used to denote an energy calculation at the *Method(E)* level with the *Basis(E)* sets for the geometry optimized at the *Method(G)* level with the *Basis(G)* sets. Here, the energetics of the B3LYP/6-31G** geometries were calculated at both the B3LYP/6-31(++)$_S$G** and frozen core CCSD/6-31G** levels.[37,38] The thermal energy ($E_{elec} + E_{vib} + E_{rot} + E_{trans}$) correction and Gibbs free energy ($H - TS$) correction of the redox process were estimated at the reoptimized geometries using the smaller STO-3G basis sets,[39a] and were included in the estimate of the reduction energy and reduction free energy calculations. The bond dissociation energy and free energy (ΔE_d and ΔG_d) of $[Fe(SCH_3)_4]^-$ into $[Fe(SCH_3)_3]^0$ and SCH_3^- and the bond association energy and free energy (ΔE_a and ΔG_a) of $[Fe(SCH_3)_3]^-$ with SCH_3^- into $[Fe(SCH_3)_4]^{2-}$ were also calculated at the B3LYP/6-31(++)$_S$G** and frozen core CCSD/6-31G** levels. Because the basis set superposition errors (BSSE) tend to cancel each other in summations of ΔE_d and ΔE_a and of ΔG_d and ΔG_a, the BSSE (<0.016 kcal/mol at the B3LYP/6-31G** level) was neglected for the thermodynamic cycle analysis. Natural bond orbital (NBO) analysis[40] and Mülliken spin population analysis were carried out at the B3LYP/6-31G** level on charge and spin populations, respectively.

All calculations were performed using the NWChem[41a] and Gaussian98[39b] program packages. The molecular orbital visualizations were performed using the extensible computational chemistry environment (Ecce) application software.[41b]

Results and Discussion

Geometries of $[Fe(SCH_3)_4]^{n-}$ (n = 0, 1, 2) and $[Fe(SCH_3)_3]^{n-}$ (n = 0, 1). Full geometry optimizations were performed using the B3LYP method with the 6-31G** basis sets, which has been shown to give good descriptions of Rd analogues.[27d] The previous benchmark study focused on the dependence of the final geometry on the DFT methods and the basis sets used for the optimization, in which good agreement with available crystal data was found.[27d] In particular, deviations of calculated Fe−S bond lengths and ∠S−Fe−S bond angles were within 0.06 Å and 3°, respectively, with respect to experimental data of $[Fe(S_2\text{-}o\text{-xyl})_2]^{2-/-}$ and $[Fe(SC_6H_2\text{-}2,4,6\text{-}t\text{-}Bu_3)_3]^-$. Here, the B3LYP/6-31G** optimized geometries of $[Fe(SCH_3)_4]^{n-}$ (n = 0, 1, 2) and $[Fe(SCH_3)_3]^{n-}$ (n = 0, 1) (Table 1) are briefly summarized and then discussed in terms of differences between the various oxidation states. The DFT calculations provide important structural information, especially about $[Fe(SCH_3)_4]^0$ and $[Fe(SCH_3)_3]^0$, because most experimental data are for the charged states $[Fe(SCH_3)_4]^{2-/-}$ and $[Fe(SCH_3)_3]^-$. In addition, a study of different spin states for $[Fe(SCH_3)_4]^0$ is presented because its ground state is not well characterized.

(a) $[Fe(SCH_3)_4]^{n-}$. The structures of the two species of the couple found in rubredoxin, $[Fe(SCH_3)_4]^{2-/-}$, are relatively well characterized. Both the oxidized and reduced species usually have high-spin ground states with $S = {}^5/_2$ and 2, respectively.[26a,d] $[Fe^{III}(SCH_3)_4]^-$ and $[Fe^{II}(SCH_3)_4]^{2-}$ favor the “D_{2d}” ML_4

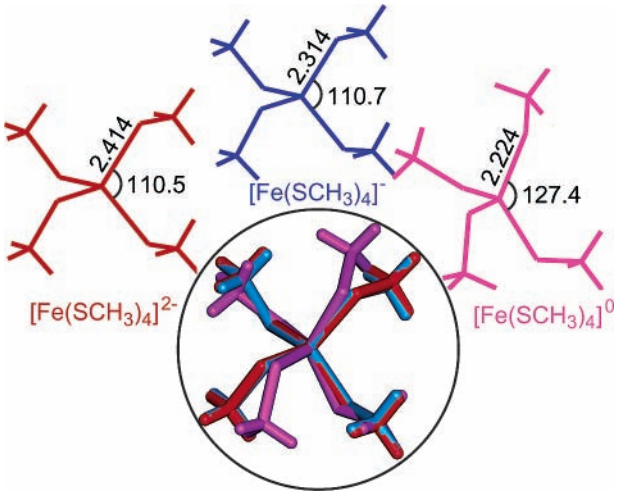

Figure 2. Schematic and superposed geometries of $[Fe(SCH_3)_4]^{2-}$ (red), $[Fe(SCH_3)_4]^{-}$ (blue), and $Fe(SCH_3)_4]^0$ (purple).

structure, which is similar to the geometry of the Rd redox site and was found to be the lowest energy conformation in a previous study.[27a] On reduction from $[Fe^{III}(SCH_3)_4]^-$ to $[Fe^{II}(SCH_3)_4]^{2-}$, the overall change in the optimized geometries is rather small (Figure 2). The major change is an increase in the Fe−S bond lengths by 0.100 Å (Table 1), in very good agreement with the experimental value of 0.089 Å for $[Fe(S_2$-*o*-xyl$)_2]^{2-/-}$.[34b] The optimized geometries of both complexes have local tetrahedral structures around the Fe with essentially no change upon reduction in the optimized ∠S−Fe−S bond angles, also in very good agreement with the experimental values.[34b]

The structure of the superoxidized $[Fe(SCH_3)_4]^0$ species is less well characterized. The present calculations indicate that this species also has a high-spin ground state ($S = 2$), which is more stable by 0.16 and 0.64 eV than the triplet ($S = 1$) and singlet ($S = 0$) states, respectively. On oxidation from $[Fe(SCH_3)_4]^-$ to the high-spin $[Fe(SCH_3)_4]^0$, the Fe−S bond lengths decrease by 0.090 Å (Figure 2 and Table 1), but the two trans ∠S−Fe−S angles (on the symmetry planes) increase by 17°. This results in a distorted tetrahedral structure (C_{2v}), which still retains some tetrahedral character because of steric crowding between the thiolate ligands (Figure 2). The distortion is due to the Jahn−Teller effect upon oxidation of the high-spin Fe^{III} center. In comparison to the high-spin $[Fe(SCH_3)_4]^0$ species, the calculated Fe−S bond lengths of the triplet and singlet $[Fe(SCH_3)_4]^0$ species are shorter by 0.077 and 0.105 Å, respectively. Both the triplet and singlet $[Fe(SCH_3)_4]^0$ structures show more tetrahedral character than the high-spin $[Fe(SCH_3)_4]^0$ with the two trans ∠S−Fe−S angles of the triplet and singlet $[Fe(SCH_3)_4]^0$ structures being about 117° and 114°, respectively.

The only experimental structural data related to $[Fe(SCH_3)_4]^0$ is for $[Fe^{IV}(\text{“}S_2\text{”})_2(PMe_3)]$ (“S_2” = 1,2-benzenedithiolate), which is a low-spin ($S = 1$) complex with a planar Fe^{IV}−S core.[34c] The calculated Fe−S bond lengths of $[Fe(SCH_3)_4]^0$ relative to this complex are slightly shorter by 0.038 Å for $S = 0$, within 0.01 Å for $S = 1$, but are slightly longer by 0.039 Å for $S = 2$. Although a search was carefully made for a structure of $[Fe(SCH_3)_4]^0$ with a planar core and either a high-spin or low-spin state, the results always smoothly converged to the tetrahedral or distorted tetrahedral core with a high-spin ground state. The low-spin state of $[Fe^{IV}(\text{“}S_2\text{”})_2(PMe_3)]$ is presumably due to structural restrictions.[34c] Because $[Fe^{III}(SCH_3)_4]^-$ has a high-spin ground state, it is expected that its photodetachment would lead to a high-spin state from a one-electron transition. It should be noted that oxidation of an $[Fe^{III}(SR)_4]^-$ site would place more geometric strain on the surrounding protein than reduction of the same site because of the greater distortion of the tetrahedral structure of the core.

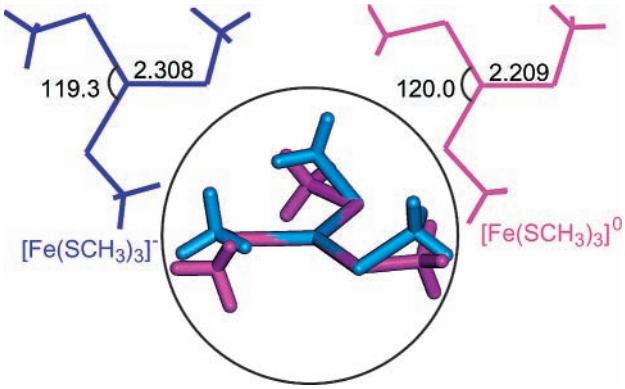

Figure 3. Schematic and superposed geometries of $[Fe(SCH_3)_2]^-$ (blue) and $Fe(SCH_3)_4]^0$ (purple).

Overall, of the three- and four-ligand redox couples, $[Fe(SCH_3)_4]^{2-/-}$ shows the least geometric distortion upon charge change. Interestingly, this is the redox couple found in the [1Fe] proteins, such as rubredoxin, desulforedoxin, desulfoferrodoxin, and rubrerythrin. It is significant to note that this redox couple would impart the least amount of strain on the protein upon change in oxidation state.

(b) $[Fe(SCH_3)_3]^{n-}$. The structures of the three-ligand $[Fe(SCH_3)_3]^{-/0}$ couple are also less well characterized experimentally. The current calculations indicate that $[Fe^{III}(SCH_3)_3]^0$ and $[Fe^{II}(SCH_3)_3]^-$ both have high-spin ground states with $S = 2$ and $^5/_2$, respectively. Experimentally, a three-coordinate complex, $[Fe^{II}(SR_3)_3]^-$ (R = 2,4,6-*t*-$Bu_3C_6H_2$), has been shown to have a “Y”-shaped distortion, which is reflected somewhat in the calculation.[34a] In the optimized structures of $[Fe(SCH_3)_3]^{-/0}$ (Figure 3), there are some interesting changes between the ferrous and ferric complexes. One change is the decrease in the Fe−S bond length by about 0.10 Å upon oxidation. Comparing Figures 2 and 3, we can see that the Fe−S bond lengths of the three-coordinate ferrous and ferric sites are shorter by about 0.10 Å than those in the four-coordinate sites. This reflects a stronger Fe−S bonding interaction in the three-coordinate $[Fe(SCH_3)_3]^{-/0}$ complexes than in the four-coordinate $[Fe(SCH_3)_4]^{2-/-}$ complexes. We also note that although the planar triangular structure in the three-coordinate complexes is well preserved on oxidation (Figure 3), the out-of-plane torsion of the SCH_3 ligands changes from 31° to 0°. The rotation of the methyl groups out of the plane in $[Fe^{II}(SCH_3)_3]^-$ reflects a weaker Fe−S π character than in $[Fe^{III}(SCH_3)_3]^0$, where the methyl groups are coplanar with the iron and the sulfurs. This rotation would also place geometric strain on the surrounding protein via the ligands connecting the core to the protein.

Electronic Structures of $[Fe(SCH_3)_4]^{n-}$ ($n = 0, 1, 2$) and $[Fe(SCH_3)_3]^{n-}$ ($n = 0, 1$). To understand the relationship between the electronic structure and the active site geometries, a simplified molecular orbital (MO) interaction diagram between a high-spin Fe and the thiolate ligands is shown in Figure 4. We have analyzed the B3LYP/6-31G** natural bond orbital (NBO) charges and Mülliken spin populations of $[Fe(SCH_3)_4]^{n-}$ ($n = 0, 1, 2$) and $[Fe(SCH_3)_3]^{n-}$ ($n = 0, 1$), as given in Table 2. The NBO charges are in good agreement with the CHelpG charges from our previous UHF calculation[27a] but are much more polarized than the CHelpG charges from a nonlocal DFT calculation.[26c] Overall, most of the unpaired electron density

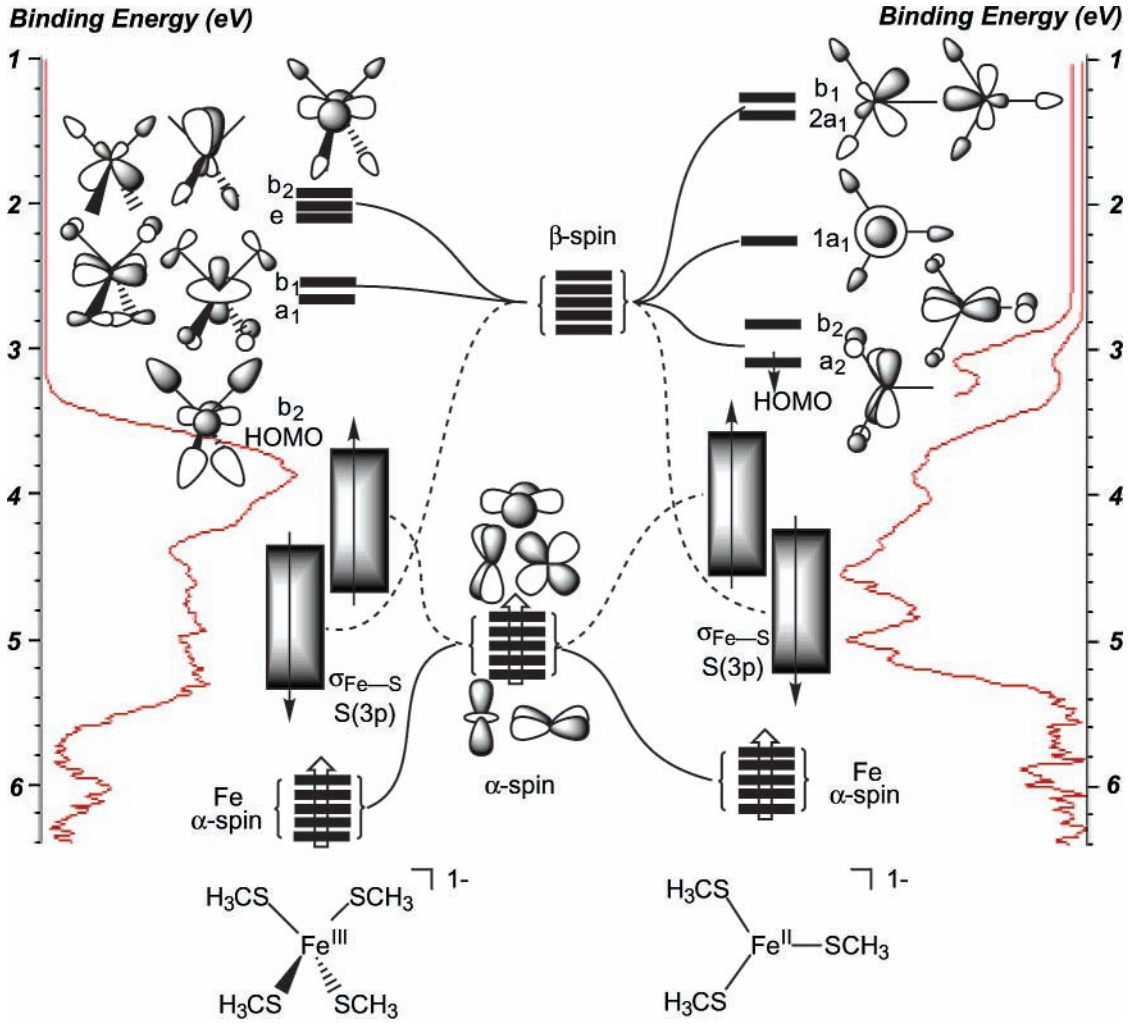

Figure 4. Schematic orbital interaction diagram for a tetrahedral D_{2d} $[Fe(SCH_3)_4]^-$ complex (the left-hand side) and a triangular C_{2v} $[Fe(SCH_3)_3]^-$ complex (the right-hand side) compared to the respective photoelectron spectra (red).

TABLE 2: Natural Bond Orbital (NBO) Charges (e) and Mülliken Spin Populations (e) at the B3LYP/6-31G Level for $[Fe(SCH_3)_4]^{2-}$, $[Fe(SCH_3)_4]^-$, $[Fe(SCH_3)_4]^0$, $[Fe(SCH_3)_3]^-$, and $[Fe(SCH_3)_3]^0$**

	NBO charges			spin populations		
	Fe	S	C	Fe	S	C
$[Fe(SCH_3)_4]^{2-}$	+1.320	−0.653	−0.809	+3.797	+0.047	−0.002
$[Fe(SCH_3)_4]^-$	+1.455	−0.504	−0.813	+4.028	+0.224	+0.006
$[Fe(SCH_3)_4]^0$	+1.347	−0.277	−0.821	+3.528	+0.102	+0.010
$[Fe(SCH_3)_3]^-$	+1.182	−0.602	−0.805	+3.701	+0.081	+0.011
$[Fe(SCH_3)_3]^0$	+1.406	−0.412	−0.810	+4.035	+0.289	+0.014

still localizes on the metal orbitals in $[Fe(SCH_3)_4]^{2-/-/0}$ and $[Fe(SCH_3)_3]^{-/0}$.

(a) $[Fe(SCH_3)_4]^{n-}$. Generally, in a roughly T_d weak ligand field of $[Fe(SCH_3)_4]^-$, the orbitals t_2 and e have a small ligand-field splitting, so that a high-spin state is favored.[27d,42] In a lower D_{2d} symmetry, the t_2 and e orbitals transform as (e, b_2) and (b_1, a_1), respectively. A strong spin exchange interaction leads to spin polarization, which splits the occupied α-spin−orbitals below the β-spin−orbitals. Consequently, although the classical electronic structure at the restricted HF level would indicate that the oxidation of $[Fe(SCH_3)_4]^-$ involves the Fe(d) electron, our broken-symmetry DFT calculations show that the interaction between Fe and the thiolate ligands leads to a less common "inverted level scheme", in which the S(3p) ligand orbitals lie below the Fe(3d) β-spin−orbitals and above the Fe(3d) α-spin−orbitals (Figure 4). Our results are consistent with previous Xα calculations[22] and with PES[16,25] and Mössbauer[43] experimental measurements.

Upon reduction from $[Fe^{III}(SCH_3)_4]^-$ to $[Fe^{II}(SCH_3)_4]^{2-}$, the extra electron enters a low-lying Fe β-spin−orbital, d_{z^2} (a_1), which has some Fe−S π* character (Figure 5a). In the ferrous complex, the Fe−S bond lengths increase with a weakening of the Fe−S π character, resulting in the electron densities from the Fe back-donating to the thiolate ligands. Consequently, even though an electron is added to the Fe d_{z^2} orbital, the reduction leads to a relatively small increase of the electron density on the Fe. The NBO charge of the Fe center decreases only by 0.135 e with a large increase of the electron density on the four S atoms so that the total NBO charge on all four S increases by a total of 0.596 e (Table 2). Meanwhile, the spin populations of the Fe and all four S decrease by 0.231 and 0.708 e, respectively. Clearly, the ligand orbital is indirectly involved in the one-electron transition of the reduction process. In other words, with the decrease of Fe−S π bonding interaction upon reduction from $[Fe^{III}(SCH_3)_4]^-$ to $[Fe^{II}(SCH_3)_4]^{2-}$, the Fe d_{z^2} (a_1) orbital with Fe−S π* character is lowered in energy, which leads to an increase in reduction potential. Furthermore, one can predict that hydrogen bonding interaction between a hydrogen donor and the high-lying β-spin Fe d_{z^2} (a_1) orbital may similarly lead to a decrease in energy for the Fe β-spin minority electron, thus increasing the reduction potential for $[Fe^{III}(SCH_3)_4]^-$.

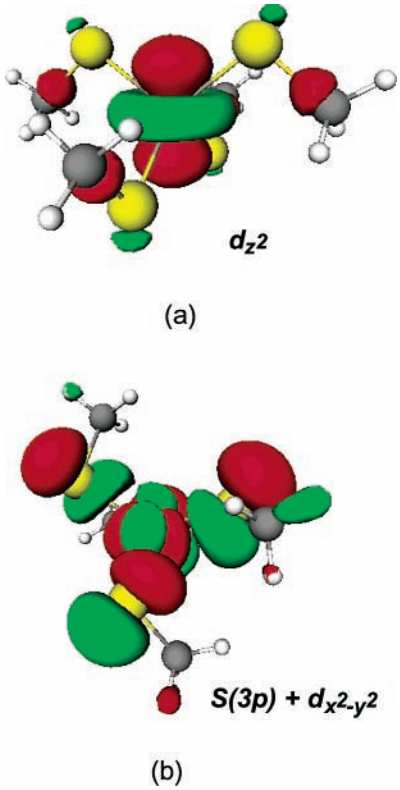

Figure 5. Molecular orbitals of (a) the reduced orbital (d_{z^2}) from $[Fe(SCH_3)_4]^-$ to $[Fe(SCH_3)_4]^{2-}$ and (b) the oxidized orbital [S(3p) + $d_{x^2-y^2}$] from $[Fe(SCH_3)_4]^-$ to $[Fe(SCH_3)_4]^0$.

On the other hand, the oxidation from $[Fe(SCH_3)_4]^-$ to $[Fe(SCH_3)_4]^0$ involves the highest-occupied near-degenerate S(3p) α-spin−orbital (b_2) with Fe−S σ^* character (Figure 5b), resulting in a strong Jahn−Teller distortion toward a planar structure. With an increase of the molecular planarity, the lowest unoccupied molecular orbital (b_2) (LUMO) of $[Fe(SCH_3)_4]^0$ rises in energy so that the Fe−S bond strength and electron density on the Fe increase. Thus, although the detached electron is mainly from the S(3p) α-spin−orbital, the geometry distortion leads to a redistribution of the charge densities on the metal center and the thiolate ligands, including the β-spin electrons. Consequently, the oxidation of $[Fe^{III}(SCH_3)_4]^-$ not only leads to a large decrease of the electron density on the four S atoms so that the total NBO charge on all four S increases by 0.908 e, but also to a significant increase of the electron density on the Fe so that the NBO charge of the Fe center decreases by 0.108 e. Here, the one-electron transition of the oxidation process indirectly involves the Fe $d_{x^2-y^2}$ orbital, unlike the reduction of $[Fe^{III}(SCH_3)_4]^-$. Overall, the spin populations of the Fe and all four S decrease by 0.500 and 0.488 e, respectively. These results are consistent with Mössbauer experiments for a series of iron sulfides, where the Fe^{IV} isomer shifts are identical with those measured for the Fe^{III} complexes.[42] Combined with previous findings of PES and ligand K-edge X-ray absorption and spectroscopy of $FeCl_4^-$,[22] the current MO assignment and PES measurements in the gas-phase further confirm the inverted level pattern of $[Fe^{III}(SCH_3)_4]^-$. Hence oxidation of the high-spin Fe^{III} redox site involves a S(3p) α-spin electron and all the intense detachment features observed between 3.4 and 5.4 eV in the 193 nm spectrum of $[Fe^{III}(SCH_3)_4]^-$ were due to the ligand S 3p α- and β-spin levels (the left-hand side of Figure 4), whereas the Fe 3d α-levels are below the ligand levels in energy and cannot be fully observed at this photon energy.[16,25]

(b) $[Fe(SCH_3)_3]^{n-}$. Similarly, in a roughly D_{3h} ligand field of the triangular $[Fe(SCH_3)_3]^{-/0}$, the Fe 3d orbitals transform into e″, a$_1$′, and e′ with a slightly larger splitting energy than that in a T_d ligand field of the tetrahedral $[Fe(SCH_3)_4]^{n-}$. However, the system still remains a high-spin ground state because thiolates are weak-field ligands. In a lower C_{2v} symmetry, these MOs transform as e′ → (a_2, b_2), a′$_1$ → 1a$_1$, and e″ → (2a$_1$, b_1).[42] Further spin exchange interaction leads to spin polarization, which splits the occupied α-spin−orbitals below the β-spin−orbitals. Consequently, the three-ligand $[Fe(SCH_3)_3]^-$ complex also exhibits an inverted level pattern, in which the S(3p) ligand orbitals lie between the Fe(3d) β- and α-spin−orbitals (the right-hand side of Figure 4).

The extra electron in $[Fe^{II}(SCH_3)_3]^-$ is located on the Fe d_{xz} (a_2) β-spin−orbital. Compared to the β-spin−orbital (a_1) of $[Fe^{II}(SCH_3)_4]^{2-}$, the β-spin−orbital (a_2) of $[Fe^{II}(SCH_3)_3]^-$ is lowered in energy by about 4 eV at the B3LYP/6-31(++)$_S$G** level because of a relatively large splitting energy in a triangular ligand field for a high-spin Fe^{II} center. This leads to a higher oxidation energy and a smaller HOMO−LUMO energy gap with respect to $[Fe^{II}(SCH_3)_4]^{2-}$, as shown in Figure 4. To decrease the antibonding Fe−S π^* interaction of the a_2 orbital, the thiolates in $[Fe^{II}(SCH_3)_3]^-$ tend to be out-of-plane. Upon oxidation of $[Fe^{II}(SCH_3)_3]^-$, the resulting $[Fe^{III}(SCH_3)_2]^0$ species favors a planar structure with an increase of π character in the Fe−S bonds. This is consistent with the fact that the oxidation from $[Fe^{II}(SCH_3)_3]^-$ to $[Fe^{III}(SCH_3)_2]^0$ involves the low-lying Fe d_{xz} (a_2) β-spin−orbital with Fe−S π^* character. The oxidation leads to a decrease of electron density on the Fe center and the three S atoms. As given in Table 2, the NBO charge of the Fe increases by 0.224 e and the total NBO charge on all three S increases by 0.570 e, whereas the spin populations of the Fe and the three S increase by 0.334 and 0.624 e, respectively. The electron donation from the thiolate ligands into the Fe 3d orbitals is again responsible for the charge density redistribution. Because $[Fe(SCH_3)_3]^{-/0}$ has fewer ligands than $[Fe(SCH_3)_4]^{2-/-}$, the oxidation of $[Fe^{II}(SCH_3)_3]^-$ to $[Fe^{III}(SCH_3)_3]^0$ leads to a greater decrease in electron density on the Fe center than that of $[Fe^{II}(SCH_3)_4]^{2-}$ to $[Fe^{III}(SCH_3)_4]^-$ because there is less back-donation from the ligands.

Vertical and Adiabatic Detachment Energies of $[Fe(SCH_3)_4]^-$ and $[Fe(SCH_3)_3]^-$. The ADE, VDE, and the oxidant relaxation energies λ_{oxd} of $[Fe(SCH_3)_4]^{-/0}$ and $[Fe(SCH_3)_3]^{-/0}$ were calculated at B3LYP and CCSD levels of theory (Table 3). A previous study made a thorough investigation on the dependence of these energies on levels of theory and basis sets.[25d] All the computed results are in good agreement with the experiment, but the CCSD/6-31G** results are generally better than the B3LYP/6-31G** results. The best results are from the B3LYP/6-31(++)$_S$G** calculations with additional diffuse functions on sulfur. Presumably, this is because the diffuse functions allow orbitals to occupy a larger region of space, which is important for systems where electrons are relatively far from the nucleus, such as molecules with lone pairs, anions, excited states, or generally systems with low ionization potentials.

From the electronic structure analysis, we see that the oxidized electron orbital of the [1Fe] redox sites usually consists of either an Fe 3d orbital with weak Fe−S π^* antibonding character for the Fe^{II} site or a S(3p) orbital with Fe−S σ^* antibonding character for the Fe^{III} site. Overall the relatively weak ligand field interaction and strong Fe−S bonding interaction between the thiolate ligands and Fe destabilize the oxidized Fe β-spin electrons. Thus, $[Fe^{II}(SCH_3)_4]^{2-}$ would be expected to have a

TABLE 3: Experimental and Calculated Adiabatic (ADE) and Vertical (VDE) Detachment Energies (eV) and the Oxidant Relaxation Energies (λ_{oxd}) (eV) for $[Fe^{II}(SCH_3)_3]^-$ and $[Fe^{III}(SCH_3)_4]^-$ at B3LYP/6-31(++)$_S$G and CCSD/6-31G** Levels Using the B3LYP/6-31G** Geometry (G_1) and the B3LYP/6-31(++)$_S$G** Geometry (G_2)**

	$[Fe(SCH_3)_3]^-$			$[Fe(SCH_3)_4]^-$		
	ADE	VDE	λ_{oxd}	ADE	VDE	λ_{oxd}
B3LYP/6-31G**//G_1	2.55	2.80	−0.25	3.28	3.58	−0.30
CCSD/6-31G**//G_1	2.66	2.96	−0.30	3.67	3.88	−0.21
B3LYP/6-31(++)$_S$G**//G_1	2.70	2.94	−0.24	3.35	3.66	−0.31
B3LYP/6-31(++)$_S$G**//G_2	2.70	2.94	−0.24	3.35	3.67	−0.32
exp[a]	2.80(±0.06)	3.08(±0.06)	−0.28(±0.08)	3.40(±0.06)	3.80(±0.06)	−0.40(±0.08)

[a] Reference 16.

SCHEME 1

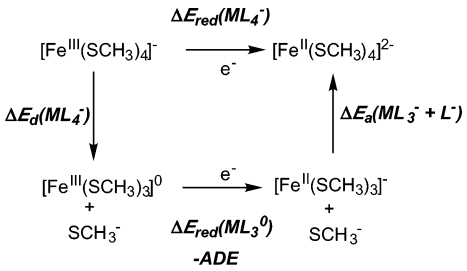

much lower electron detachment energy than $[Fe^{II}(SCH_3)_3]^-$. On the other hand, even though the high-spin d^5 electron configuration of Fe^{III} is particularly stable in a tetrahedral ligand field, $[Fe^{III}(SCH_3)_4]^-$ has a detachment energy similar to $[Fe^{II}(SCH_3)_3]^-$ with the high-spin d^6 electron configuration of Fe^{II}. This is because $[Fe^{III}(SCH_3)_4]^-$ has more destabilization by ligand interactions in a weaker ligand field than $[Fe^{II}(SCH_3)_3]^-$, with a net result of similar detachment energies. Unlike the thiolate ligands, weaker σ- and π-donor ligands stabilize the Fe^{II} minority β-spin electron and the S(3p) α-spin electrons. For instance, weaker donor ligands such as Cl^- and SCN^- interact with Fe^{II} or Fe^{III} to generate higher oxidation energies with respect to the stronger donor ligand, SCH_3^-.[16,25]

Our previous PES studies of the Fe^{II}/Fe^{III} redox couple revealed that the Fe^{II} site can be easily oxidized to Fe^{III}, whereas the latter is much more difficult to be oxidized further because the oxidized electron involves a low-lying S(3p) α-spin electron rather than a low-lying Fe β-spin electron.[16,25] For instance, the ADEs of $[Fe^{III}(SCH_3)_4]^-$ and $[Fe^{III}Cl_4]^-$ are larger by 0.60 and 1.80 eV, respectively, than those of $[Fe^{II}(SCH_3)_3]^-$ and $[Fe^{II}Cl_3]^-$. Our theoretical ADE for $[Fe^{III}(SCH_3)_4]^-$ is larger by 0.65 eV than that of $[Fe^{II}(SCH_3)_3]^-$ at the B3LYP/6-31(++)$_S$G** level, which is in excellent agreement with the experimental results (Table 3). The strong Jahn−Teller distortion in the Fe^{III}/Fe^{IV} couple is reflected in the λ_{oxd} of $[Fe^{III}(SCH_3)_4]^-$, which is larger in magnitude than that of $[Fe^{II}(SCH_3)_3]^-$ by 0.12 eV experimentally. The B3LYP/6-31(++)$_S$G** energy calculations are in good agreement with a value of 0.08 eV.

Intrinsic Reduction Potential of $[Fe(SCH_3)_4]^{-/2-}$. The $Fe(SCH_3)_4]^{2-/-}$ redox couple is equivalent to the biologically relevant couple of Rd. However, because the tetrathiolate Fe^{II} species is not stable, the experimental electron detachment energy of $[Fe(SCH_3)_4]^{2-/-}$ in the gas-phase cannot be obtained. We carried out a computational study of the reduction potential energy $\Delta E_{red}(ML_4^-)$ and free energy $\Delta G_{red}(ML_4^-)$ for $[Fe(SCH_3)_4]^-$ in combination with the available PES data. As shown in Scheme 1, the energy (and the free energy) for the reduction process from $[Fe(SCH_3)_4]^-$ to $[Fe(SCH_3)_4]^{2-}$ can be regarded as equal, via a thermodynamic cycle, to that for the dissociation of $[Fe(SCH_3)_4]^-$ into $[Fe(SCH_3)_3]^0$ and SCH_3^-, followed by the reduction of $[Fe(SCH_3)_3]^0$, and finally the association of $[Fe(SCH_3)_3]$- with SCH_3^- to form $[Fe(SCH_3)_4]^{2-}$. Thus, the reduction energy of $[Fe(SCH_3)_4]^-$, $\Delta E_{red}(ML_4^-)$, is equal to

$$\Delta E_{red}(ML_4^-) = \Delta E_d(ML_4^-) - ADE + \Delta E_a(ML_3^- + L^-) \quad (4)$$

where ADE is the experimental oxidation energy of $[Fe(SCH_3)_3]^-$, $\Delta E_d(ML_4^-)$ is the bond dissociation energy of $[Fe(SCH_3)_4]^-$ to $[Fe(SCH_3)_3]^0$ and SCH_3^-, and $\Delta E_a(ML_3^- + L^-)$ is the bond association energy of $[Fe(SCH_3)_3]^-$ with SCH_3^- into $[Fe(SCH_3)_4]^{2-}$. If the bond dissociation and association energies ΔE_d and ΔE_a are available from experiments, this would give an experimental value for $\Delta E_{red}(ML_4^-)$. Otherwise, these energies can be obtained via quantum mechanical calculations. Furthermore, the reduction free energy of $[Fe(SCH_3)_4]^-$, $\Delta G_{red}(ML_4^-)$, can be written as

$$\Delta G_{red}(ML_4^-) = \Delta G_d(ML_4^-) + [-ADE + T(R - \Delta S)] + \Delta G_a(ML_3^- + L^-) \quad (5)$$

R is the gas constant, $T\Delta S$ is the entropic contribution, and $\Delta G_d(ML_4^-)$ and $\Delta G_a(ML_3^- + L^-)$ are the relevant dissociation and association energies, respectively. In principle, theoretical calculations can give a good description of the summation of ΔE_d and ΔE_a (ΔE_{d+a}) and of ΔG_d and ΔG_a (ΔG_{d+a}), because of the cancellation of BSSE, as well as the systematic error cancellation of the computational methods. Thus, estimates based on reasonable calculations and the experimental ADE (2.80 eV)[16] of $[Fe(SCH_3)_3]^-$ should yield reasonably accurate reduction energies and free energies of $[Fe(SCH_3)_4]^-$.

Table 4 summarizes the calculated reduction energies and free energies of $[Fe(SCH_3)_4]^-$, the calculated dissociation energies and free energies of $[Fe(SCH_3)_4]^-$, and the calculated SCH_3^- association energies and free energies of $[Fe(SCH_3)_3]^-$. $\Delta E_{red}^{calc}(ML_4^-)$ and $\Delta G_{red}^{calc}(ML_4^-)$ are the calculated reduction energy and free energy of the $[Fe(SCH_3)_4]^{-/2-}$ redox couple from energy calculations of $[Fe(SCH_3)_4]^{-/2-}$. $\Delta E_{red}^{"exp"}$ and $\Delta G_{red}^{"exp"}$ are the estimated experimental reduction energy and free energy utilizing the experimental value of the ADE of the $[Fe(SCH_3)_3]^{-/0}$ couple and calculated values of ΔE_{d+a}, ΔG_{d+a}, and $T\Delta S$ in eqs 4 and 5. In addition, the reduction energies $[\Delta E_{red}^{calc}(ML_4^-)]$ and free energies $[\Delta G_{red}^{calc}(ML_4^-)]$ were computed using a theoretical value of the ADE of the $[Fe(SCH_3)_3]^{-/0}$ couple and the theoretical values of ΔE_{d+a}, ΔG_{d+a}, and $T\Delta S$ in eqs 4 and 5, which gave nearly identical results as $\Delta E_{red}^{"exp"}$ and $\Delta G_{red}^{"exp"}$. This indicates that the accumulation of errors in utilizing eqs 4 and 5 to evaluate ΔE_{red}^{calc} and ΔG_{red}^{calc} can be neglected. Our computational results also show that the thiolate dissociation of $[Fe(SCH_3)_4]^{2-}$ is exothermic by 2.0−2.3 eV, i.e., $[Fe(SCH_3)_4]^{2-}$ is very unstable as an isolated species. This result is consistent with our previous experimental observation[16] and explains why the PES spectra of $[Fe(SCH_3)_4]^{2-}$ could not be obtained experi-

TABLE 4: Calculated and Estimated Reduction Energies and Reduction Free Energies, $\Delta E_{red}^{calc}(ML_4^-)$, $\Delta E_{red}^{"exp"}(ML_4^-)$, $\Delta G_{red}^{calc}(ML_4^-)$, and $\Delta G_{red}^{"exp"}(ML_4^-)$, of $[Fe(SCH_3)_4]^-$, Calculated SCH_3^- Dissociation Energies and Free Energies, $\Delta E_d(ML_4^-)$ and $\Delta G_d(ML_4^-)$, of $[Fe(SCH_3)_4]^-$, and Calculated SCH_3^- Association Energies and Free Energies, $\Delta E_a(ML_3^- + L^-)$ and $\Delta G_a(ML_3^- + L^-)$, of $[Fe(SCH_3)_3]^-$ Using the B3LYP/6-31G Geometry (G_1) and the B3LYP/6-31(++)$_S$G** Geometry (G_2) (All Energies in eV)**

	ΔE_{red}^{calc}	ΔG_{red}^{calc}	$\Delta E_{red}^{"exp"}$	$\Delta G_{red}^{"exp"}$	ΔE_a	ΔG_a	ΔE_d	ΔG_d
B3LYP/6-31G**	2.037	2.170	1.79	1.92	1.654	2.148	2.933	2.497
CCSD/6-31G**//G_1	2.029	2.162	1.88	2.02	1.487	1.981	3.197	2.761
B3LYP/6-31(++)$_S$G**//G_1	1.747	1.880	1.64	1.78	1.807	2.301	2.637	2.201
B3LYP/6-31(++)$_S$G**	1.740	1.873	1.64	1.77	1.803	2.297	2.635	2.199

mentally. It also reflects that the high-spin Fe^{II} site favors a three-coordinated structure, whereas the high-spin Fe^{III} site favors a four-coordinated one. Thus, the $Fe^{II}-Fe^{III}$ conversion may play a key role in the rich Fe−S cluster chemistry and biochemistry, which involves the formation and breaking of Fe−S bonds.[43,44]

Overall, the calculated values of the energies were close to the estimated experimental values but were about 0.1−0.2 eV higher. The results for the B3LYP/6-31(++)$_S$G** energy calculations are almost identical whether the B3LYP/6-31G** or B3LYP/6-31(++)$_S$G** geometry is used,[27d] so all calculations presented here are for the B3LYP/6-31G** geometry. The ΔE_{red}^{calc} range from 1.74 to 2.04 eV. In previous studies, Noodleman and co-workers predicted a ΔE_{red}^{calc} of 1.79 eV from DFT calculations at the local density approximation (LDA),[26c] whereas Ichiye and co-workers predicted a ΔE_{red}^{calc} of 2.14 eV from unrestricted Hartree−Fock (UHF) calculations using an aug-TVZ basis set.[27] The new calculations fall in the same range. Using the experimental ADE (2.80 eV) of $[Fe(SCH_3)_3]^-$, we obtained the "experimental" estimate of the reduction energy $\Delta E_{red}^{"exp"}$, ranging from 1.64 to 1.88 eV with the calculated ΔE_{d+a} values ranging from 4.44 to 4.70 eV. Interestingly, the B3LYP/6-31(++)$_S$G** energy calculations give ΔE_{red}^{calc} that are about 0.3 eV lower than the B3LYP/6-31G** or the CCSD/6-31G** and a higher ΔE_a and lower ΔE_d than the B3LYP/6-31G** or the CCSD/6-31G**. The reason is that adding more diffuse functions leads to an increase of the bonding interaction between Fe and SCH_3^-. Consequently, the tetracoordinated $[Fe(SCH_3)_4]^{-/2-}$ are stabilized more than the three coordinated $[Fe(SCH_3)_3]^{0/-}$ in comparison to the calculations using the 6-31G** basis set. In addition, the B3LYP/6-31(++)$_S$G** energy calculation gives the most consistent results for the ΔE_{red}^{calc} and $\Delta E_{red}^{"exp"}$. Because the B3LYP/6-31(++)$_S$G** energy calculation also gives very good descriptions of the ADE, VDE, and λ_{oxd} values for $[Fe(SCH_3)_4]^-$ and $[Fe(SCH_3)_3]^-$, the B3LYP/6-31(++)$_S$G** calculated reduction energy of 1.75 eV is viewed as the best calculated value. Furthermore, this agrees with the prediction in the previous section that $[Fe^{II}(SCH_3)_4]^{2-}$ with more ligands should have a much lower electron detachment energy than $[Fe^{II}(SCH_3)_3]^-$ because the ADE of $[Fe^{II}(SCH_3)_4]^{2-}$ is −1.75 eV by calculation and −1.64 eV by the thermodynamic cycle with experimental data.

Conclusions

The electronic structure and energetics of rubredoxin redox site analogues have been elucidated here using molecular orbital theory and experimental PES data. Full geometry optimizations and energy calculations of the Rd redox site analogues, $[Fe(SCH_3)_4]^{2-/-/0}$ and $[Fe(SCH_3)_3]^{-/0}$, were performed using the B3LYP/6-31G**, B3LYP/6-31(++)$_S$G**//B3LYP/6-31G**, and CCSD/6-31G**//B3LYP/6-31G** methods. The calculations give good descriptions of the structural, electronic, and energetic properties of the [1Fe] redox sites.

The B3LYP/6-31G** calculations predict geometries for $[Fe(SCH_3)_4]^{2-/-}$ and $[Fe(SCH_3)_3]^-$ that are in good agreement with crystallographic structures for similar compounds. We further predicted geometries for the final products of the PES studies, $[Fe(SCH_3)_4]^0$ and $[Fe(SCH_3)_3]^0$, for which there are no experimental structural data. We found that for all of the redox couples studied, oxidation always results in a decrease in the Fe−S bond lengths by about 0.1 Å. The $[Fe(SCH_3)_4]^{2-/-}$ couple shows the least geometric distortion, whereas the $[Fe(SCH_3)_4]^{-/0}$ couple shows a distortion toward planarity in the four-ligand Fe−S core upon oxidation and the $[Fe(SCH_3)_3]^{-/0}$ couple shows a rotation of the methyl groups into the plane of the three-ligand Fe−S core upon oxidation. Our results thus suggest that the $[Fe(SCH_3)_4]^{2-/-}$ redox couple found in Rd would impart the least amount of strain on the surrounding protein upon change in redox states.

Our theoretical analyses combined with experimental results provide a better understanding of the electronic structure and how it leads to the geometric and energetic changes upon change in redox states. The current results support the inverted level scheme for [1Fe] Fe−S complexes. We show that the oxidations of $[Fe(SCH_3)_4]^{2-}$ and $[Fe(SCH_3)_3]^-$ involve an Fe 3d β-spin electron, whereas the oxidation of $[Fe(SCH_3)_4]^-$ involves a degenerate S(3p) orbital with a strong antibonding Fe−S σ^* character. Thus, the oxidation of $[Fe(SCH_3)_4]^-$ exhibits a strong Jahn−Teller distortion whereas the oxidation of $[Fe(SCH_3)_4]^{2-}$ shows little distortion of the tetrahedral structure leading to smaller reorganization energies for the latter. On oxidation from Fe^{II} to Fe^{III} and from Fe^{III} to Fe^{IV} of $[Fe(SCH_3)_4]^{n-}$, the charge density on the Fe from the NBO analyses changes only slightly due to charge redistribution from the ligands to the Fe. Moreover, the $Fe^{II}-Fe^{III}$ couple of $[Fe(SCH_3)_3]^{n-}$ has a much higher reduction potential than that of $[Fe(SCH_3)_4]^{n-}$ because $[Fe(SCH_3)_3]^-$ has a more stable Fe β-spin electron than $[Fe(SCH_3)_4]^{2-}$. Consequently, the stable states in the gas phase are a high-spin d^5 $[Fe^{III}(SCH_3)_4]$- and a high-spin d^6 $[Fe^{II}(SCH_3)_3]^-$.

We also predicted redox energies for redox site analogues that are not available experimentally. Calculations at the B3LYP/6-31(++)$_S$G** level predict that the oxidation energies of $[Fe(SCH_3)_4]^-$ and $[Fe(SCH_3)_3]^-$ are 3.35 and 2.70 eV, respectively, which are in very good agreement with the corresponding PES data. We also obtained computationally the reduction energy of $[Fe(SCH_3)_4]^-$ to be 1.75 eV. This value is in good agreement with that (1.64 eV) estimated using the calculated $Fe-SCH_3$ bonding energies in $[Fe(SCH_3)_4]^-$ and $[Fe(SCH_3)_4]^{2-}$ and the experimental ADE of $[Fe(SCH_3)_3]^-$ in a thermodynamic cycle. Our computational results also show that the thiolate dissociation of $[Fe^{II}(SCH_3)_4]^{2-}$ is exothermic by 2.0−2.3 eV, whereas the thiolate association of $[Fe^{III}(SCH_3)_3]^0$ is exothermic by 2.2−2.8 eV. The dependence of the coordination energetics of Fe on its valence state may play a role in the rich Fe−S cluster chemistry and biochemistry. This work demonstrates the possibility of obtaining reliable oxidation potentials of an

experimentally unstable ML_n^{2-} species from M−L bonding energies in $ML_n^{2-/-}$ and the detachment energy of $ML_{(n-1)}^{-}$.

Acknowledgment. This work was supported by grants from the National Institute of Health (GM45303 to T.I. and GM63555 to L.S.W.). We thank Prof. M. T. Werth and M. A. Walters for communicating to us the reduction potential data of the inorganic model complexes on the rubredoxin redox sites before publication and helpful discussions. Computing time was partially provided through a grant from the Molecular Science Computing Facility in the W. R. Wiley Environmental Molecular Sciences Laboratory at the Pacific Northwest National Laboratory (PNNL), sponsored by the Office of Biological and Environmental Research of the U. S. Department of Energy. PNNL is a multiprogram national laboratory operated for the U. S. Department of Energy by Battelle Memorial Institute under contract DE-AC06-76RLO 1830. T.I. also thanks Dr. Bernard R. Brooks at NIH for his hospitality while completing this manuscript.

Supporting Information Available: Supplemental tables (S1 and S2) of the calculated adiabatic and vertical detachment energies, oxidant reorganization energies, reduction energies, and reduction free energies for $[Fe(SCH_3)_4]^-$ and $[Fe(SCH_3)_3]^-$ at different levels of theory and basis sets. These materials are available free of charge via the Internet at http://pubs.acs.org.

References and Notes

(1) Gray, H. B.; Ellis, W. R., Jr. Electron Transfer. In *Bioinorganic Chemistry*; Bertini, I., Gray, H. B., Lippard, S. J., Valentine, J. S., Eds.; University Science Books: Mill Valley, CA, 1994; p 315.

(2) Frey, M. *Structure and Bonding*; Springer-Verlag: Berlin Heidelberg, 1998; Vol. 90, p 97.

(3) (a) Ichiye, T. Computational Studies of Redox Potentials of Electron-Transfer Proteins. In *Simulation and Theory of Electrostatic Interactions in Solution*; Pratt, L. R., Hummer, G., Eds.; American Institute of Physics: New York, 1999; p 431. (b) Ichiye, T. Simulations of Electron-Transfer Proteins. In *Computational Biochemistry and Biophysics*; Becker, O. M., MacKerell, A. D., Roux, B., Watanabe, M., Eds.; Marcel Dekker Inc.: New York, 2000; p 393.

(4) Adman, E. T. *Biochim. Biophys. Acta* **1979**, *549*, 107.

(5) Meyer, T. E. *Biochim. Biophys. Acta* **1989**, *975*, 1.

(6) Zeng, Q.; Smith, E. T.; Kurtz, D. M.; Scott, R. A. *Inorg. Chim. Acta* **1996**, *242*, 245.

(7) Shen, B.; Jolie, D. R.; Strout, C. D.; Diller, T. C.; Armstrong, F. A.; Gorst, C. M.; La Mar, G. N.; Stephens, P. J.; Burgess, B. K. *J. Biol. Chem.* **1994**, *269*, 8564.

(8) (a) Cammack, R. *Adv. Inorg. Chem.* **1992**, *38*, 281. (b) Tsibris, J. C. M.; Woody, R. W. *Coord. Chem. Rev.* **1992**, *38*, 281.

(9) Holm, R. H. In *Advances in Inorganic Chemistry*; Cammack, R., Ed.; Academic Press: San Diego, 1992; Vol. 38, p 1.

(10) (a) Lovenberg, W.; Sobel, B. *Proc. Natl. Acad. Sci. U.S.A.* **1965**, *54*, 193. (b) Moura, I.; Brushci, M.; Moura, J. J. G.; Xavier, A. V. *Biochem. Biophys. Res. Commun.* **1977**, *75*, 1037. (c) Moura, I.; Tavares, P.; Moura, J. J. G. *Methods Enzymol.* **1994**, *243*, 216. (d) Moura, I.; Pereira, A.; Tavares, P.; Moura, J. J. G. in *Advances in Inorganic Chemistry*; Cammack, R., Ed.; Academic Press: San Diego, 1999; Vol. 47, p 361.

(11) (a) Eggink, G.; Engel, H.; Vriend, G.; Terpstra, P.; Witholt, B. *J. Mol. Biol.* **1990**, *212*, 135. (b) Gomes, C. M.; Silva, G.; Oliveira, S.; LeGall, J.; Liu, M. Y.; Xavier, A. V.; Rodrigues-Pousada, C.; Teixeira, M. *J. Mol. Biol.* **1997**, *272*, 22502.

(12) Emerson, J. P.; Coulter, E. D.; Cabelli, D. E.; Phillips, R. S.; Kurtz, D. M., Jr. *Biochemistry* **2002**, *41*, 4348.

(13) (a) Eidsness, M. K.; Burden, A. E.; Richie, K. A.; Kurtz, Jr. D. M.; Scott, R. A.; Smith, E. T.; Ichiye, T.; Beard, B.; Min, T.-P.; Kang, C.-H. *Biochemistry* **1999**, *38*, 14803. (b) Min, T.-P.; Ergenekan, C. E.; Eidsness, M. K.; Ichiye, T.; Kang, C.-H. *Protein Sci.* **2001**, *10*, 463.

(14) (a) Hagen, K. S.; Holm, R. H. *J. Am. Chem. Soc.* **1982**, *104*, 5496. (b) Lane, R. W.; Ibers, J. A.; Frankel, R. B.; Papaefthymiou, G. C.; Holm, R. H. *J. Am. Chem. Soc.* **1977**, *99*, 84. (c) Laskowski, E. J.; Frankel, R. B.; Gillum, W. O.; Papaefthymiou, G. C.; Renaud, J.; Ibers, J. A.; Holm, R. H. *J. Am. Chem. Soc.* **1978**, *100*, 5322. (d) Holm, R. H.; Ibers, J. A. In *Iron−Sulfur Proteins*; Lovenberg, W., Ed.; Academic Press: New York, 1977; Vol. 3, p 205. (e) Werth, M. T.; Kurtz, D. M.; Howes, B. D.; Huynh, B. H. *Inorg. Chem.* **1989**, *28*, 1357. (f) Coucouvanis, D.; Swenson, D.; Baenziger, N. C.; Holah, D. G.; Kostikas, A.; Simopoulos, A.; Petrouleas, V. *J. Am. Chem. Soc.* **1976**, *98*, 5721. (g) Coucouvanis, D.; Swenson, D.; Baenzinger, N. C.; Murphy, C.; Holah, D. G.; Sfarnas, N.; Simopoulos, A.; Kostikas, A. *J. Am. Chem. Soc.* **1981**, *103*, 3350. (h) Swenson, D.; Baenziger, N. C.; Coucouvanis, D. *J. Am. Chem. Soc.* **1978**, *100*, 1932. (i) MacDonnell, F. M.; Ruhlandt-Senge, K.; Ellison, J. J.; Holm, R. H.; Power, P. P. *Inorg. Chem.* **1995**, *34*, 1815.

(15) Reiss, H.; Heller, A. *J. Phys. Chem.* **1985**, *89*, 4207.

(16) Wang, X. B.; Wang, L. S. *J. Chem. Phys.* **2000**, *112*, 6959.

(17) (a) Swartz, P. D.; Beck, B. W.; Ichiye, T. *Biophys. J.* **1996**, *71*, 2958. (b) Ergenekan, C.; Ichiye, T. Unpublished work.

(18) (a) Gupta, N.; Bonomi, F.; Kurtz, D. M., Jr.; Ravi, N.; Wang, D. L.; Huynh, B. H. *Biochemistry* **1995**, *34*, 3310. (b) de Maré, F.; Kurtz, D. M., Jr.; Nordlund, P. *Nat. Struct. Biol.* **1996**, *3*, 539.

(19) (a) Holm, R. H.; Kennepohl, P.; Solomon, E. I. *Chem. Rev.* **1996**, *96*, 2239. (b) Werth, M. T. Personal communication. (c) Bose, K.; Huang, J.; Haggerty, B. S.; Rheingold, A. L.; Salm, R. J.; Walters, M. A. *Inorg. Chem.* **1997**, *36*, 4596.

(20) (a) Yang, Y.; Beck, B. W.; Shenoy, V. S.; Ichiye, T. *J. Am. Chem. Soc.* **1993**, *115*, 7439. (b) Yelle, R. B.; Park, N. S.; Ichiye, T. *Proteins* **1995**, *22*, 154. (c) Swartz, P. D.; Ichiye, T. *Biochemistry* **1996**, *35*, 13772.

(21) Marcus, R. A.; Sutin, N. *Biochim. Biophys. Acta* **1985**, *811*, 265.

(22) (a) Butcher, K. D.; Didziulis, S. V.; Briat, B.; Solomon, E. I. *J. Am. Chem. Soc.* **1990**, *112*, 2231. (b) Butcher, K. D.; Gebhard, M. S.; Solomon, E. I. *Inorg. Chem.* **1990**, *29*, 2067. (c) Rose, K.; Shadle, S. E.; Eidsness, M. K.; Kurtz, D. M. Jr.; Scott, R. A.; Hedman, B.; Hodgson, K. O.; Solomon, E. I. *J. Am. Chem. Soc.* **1998**, *120*, 10743.

(23) (a) Wang, L. S.; Ding, C. F.; Wang, X. B.; Barlow, S. E. *Rev. Sci. Instrum.* **1999**, *70*, 1957, (b) Wang, X. B.; Ding, C. F.; Wang, L. S. *Phys. Rev. Lett.* **1998**, *81*, 3551, (c) Wang, L. S.; Ding, C. F.; Wang, X. B.; Nicholas, J. B. *Phys. Rev. Lett.* **1998**, *81*, 2667, (d) Ding, C. F.; Wang, X. B.; Wang, L. S. *J. Chem. Phys.* **1999**, *110*, 3635, (e) Wang, X. B.; Ding, C. F.; Nicholas, J. B.; Dixon, D. A.; Wang, L. S. *J. Phys. Chem. A* **1999**, *103*, 3423, (f) Wang, X. B.; Wang, L. S. *Phys. Rev. Lett.* **1999**, *83*, 3402, (g) Wang, X. B.; Wang, L. S. *Nature* (London) **1999**, *400*, 245.

(24) (a) Wang, X. B.; Wang, L. S. *J. Chem. Phys*. **1999**, *111*, 4497. (b) Wang, X. B.; Wang, L. S. *Phys. Rev. Lett*. **1999**, *83*. 3402. (c) Wang, X. B.; Wang, L. S. *J. Am. Chem. Soc*. **2000**, *122*, 2096. (d) Wang, X. B.; Wang, L. S. *J. Am. Chem. Soc.* **2000**, *122*, 2339.

(25) Yang, X.; Wang, X. B.; Fu, Y. J.; Wang, L. S. *J. Phys. Chem. A* **2003**, *107*, 1703.

(26) (a) Norman, J. G., Jr.; Ryan, P. B.; Noodleman, L. *J. Am. Chem. Soc.* **1980**, *102*, 4279. (b) Noodleman, L.; Norman, J. G., Jr.; Osborne, J. H.; Aizman, A.; Case, D. A. *J. Am. Chem. Soc.* **1985**, *107*, 3418. (c) Mouesca, J.-M.; Chen, J. L.; Noodleman, L.; Bashford, D.; Case, D. A. *J. Am. Chem. Soc.* **1994**, *116*, 11898. (d) Noodleman, L.; Peng, C. Y.; Case, D. A.; Mouesca, J.-M. *Coord. Chem. Rev.* **1995**, *144*, 199.

(27) (a) Koerner, J. B.; Ichiye, T. *J. Phys. Chem. B* **1997**, *101*, 3633. (b) Beck, B. W.; Koerner, J. B.; Ichiye, T. *J. Phys. Chem. B* **1999**, *104*, 8006. (c) Koerner, J. B.; Ichiye, T. *J. Phys. Chem. B* **2000**, *104*, 2424. (d) Niu, S.-Q.; Nichols, J. A.; Ichiye, T. *J. Phys. Chem. B*, submitted for publication.

(28) (a) Monard, G.; Merz, K. M., Jr. *Acc. Chem. Res.* **1999**, *32*, 904. (b) Sigfridsson, E.; Olsson, M. H. M.; Ryde, U. *Inorg. Chem.* **2001**, *40*, 2509.

(29) (a) Parr, R. G.; Yang, W. *Density-Functional Theory of Atoms and Molecules*, Oxford University Press: Oxford, U.K., 1989. (b) Cohen, A. J.; Handy, N. C. *Chem. Phys. Lett* **2000**, *316*, 160.

(30) Niu, S.-Q.; Hall, M. B. *Chem. Rev.* **2000**, *100*, 353.

(31) (a) Becke, A. D. *Phys. Rev.* **1988**, *A38*, 3098. (b) Becke, A. D. *J. Chem. Phys.* **1993**, *98*, 1372. (c) Becke, A. D. *J. Chem. Phys.* **1993**, *98*, 5648.

(32) Lee, C.; Yang, W.; Parr, R. G. *Phys. Rev.* **1988**, *B37*, 785.

(33) (a) Perdew, J. P. *Phys. Rev. B* **1986**, *33*, 8822. (b) Perdew, J. P.; Wang, Y. *Phys. Rev. B* **1992** *45*, 13244. (c) Becke, A. D. *J. Chem. Phys.* **1992**, *98*, 1372.

(34) (a) MacDonnell, F. M.; Ruhlandt-Senge, K.; Ellison, J. J.; Holm, R. H.; Power, P. P. *Inorg. Chem.* **1995**, *34*, 1815. (b) Lane, R. W.; Ibers, J. A.; Frankel, R. B.; Papaefthymiou, G. C.; Holm, R. H. *J. Am. Chem. Soc.* **1977**, *99*, 84. (c) Sellmann, D.; Geck, M.; Knoch, F.; Ritter, G.; Dengler, J. *J. Am. Chem. Soc.* **1991**, *113*, 3819. (d) Sellmann, D.; Becker, T.; Knoch, F. *Chem. Ber.* **1996**, *129*, 509.

(35) (a) Rassolov, V.; Pople, J. A.; Ratner, M.; Windus, T. L. *J. Chem. Phys.* **1998**, *109*, 1223. (b) Francl, M. M.; Petro, W. J.; Hehre, W. J.; Binkley, J. S.; Gordon, M. S.; DeFrees, D. J.; Pople, J. A. *J. Chem. Phys.* **1982**, *77*, 3654. (c) Hariharan, P. C.; Pople, J. A. *Theor. Chim. Acta* **1973**, *28*, 213.

(36) (a) Clark, T.; Chandrasekhar, J.; Schleyer, P. v. R. *J. Comput. Chem.* **1983**, *4*, 294. (b) Krishnam, R.; Binkley, J. S.; Seeger, R.; Pople, J. A. *J. Chem. Phys.* **1980**, *72*, 650. (c) Gill, P. M. W.; Johnson, B. G.; Pople, J. A.; Frisch, M. J. *Chem. Phys. Lett.* **1992**, *197*, 499.

(37) (a) Cizek, J. *Adv. Chem. Phys.* **1969**, *14*, 35. (b) Purvis, G. D.; Bartlett, R. J. *J. Chem. Phys.* **1982**, *76*, 1910. (c) Scuseria, G. E.; Janssen,

C. L.; Schaefer, H. F., III. *J. Chem. Phys.* **1988**, *89*, 7382. (d) Scuseria, G. E.; Schaefer, H. F., III. *J. Chem. Phys.* **1989**, *90*, 3700. (e) Pople, J. A.; Head-Gordon, M.; Raghavachari, K. *J. Chem. Phys.* **1987**, *87*, 5968.

(38) (a) Gauss, J.; Cremer, C. *Chem. Phys. Lett.* **1889**, *150*, 280. (b) Salter, E. A.; Trucks, G. W.; Bartlett, R. J. *J. Chem. Phys.* **1989**, *90*, 1752.

(39) (a) Foresman, J. B.; Frish, A. E. *Exploring Chemistry with Electronic Structure Methods*; Gaussian, Inc.: Pittsburgh, PA, 1993. (b) Frisch, M. J.; Trucks, G. W.; Schlegel, H. B.; Scuseria, G. E..; Robb, M. A.; Cheeseman, J. R.; Zakrzewski, V. G.; Montgomery, J. A.; Stratmann, R. E.; Burant, J. C.; Dapprich, S.; Millam, J. M.; Daniels, A. D.; Kudin, K. N.; Strain, M. C.; Farkas, O.; Tomasi, J.; Barone, V.; Cossi, M.; Cammi, R.; Mennucci, B.; Pomelli, C.; Adamo, C.; Clifford, S.; Ochterski, J.; Petersson, G. A.; Ayala, P. Y.; Cui, Q.; Morokuma, K.; Malick, D. K.; Rabuck, A. D.; Raghavachari, K.; Foresman, J. B.; Cioslowski, J.; Ortiz, J. V.; Stefanov, B. B.; Liu, G.; Liashenko, A.; Piskorz, P.; Komaromi, I.; Gomperts, R.; Martin, R. L.; Fox, D. J.; Keith, T.; Al-Laham, M. A.; Peng, C. Y.; Nanayakkara, A.; Gonzalez, C.; Challacombe, M.; Gill, P. M. W.; Johnson, B. G.; Chen, W.; Wong, M. W.; Andres, J. L.; Head-Gordon, M.; Replogle, E. S.; Pople, J. A. *Gaussian 98*, revision A.6; Gaussian, Inc.: Pittsburgh, PA, 1998.

(40) Glendening, E. D.; Badenhoop, J. K.; Reed, A. E.; Carpenter, J. E.; Weinhold, F. *NBO 4.M*; Theoretical Chemistry Institute, University of Wisconsin: Madison, 1999.

(41) (a) Bernholdt, D. E.; Apra, E.; Fruchtl, H. A.; Guest, M. F.; Harrison, R. J.; Kendall, R. A.; Kutteh, R. A.; Long, X.; Nicholas, J. B.; Nichols, J. A.; Taylor, H. L.; Wong, A. T.; Fann, G. I.; Littlefield, R. J.; Nieplocha, J. *Int. J. Quantum Chem. Symposium* **1995**, *29*, 475. (b) Black, G.; Chase, J.; Didier, B.; Feller, D.; Gracio, D.; Jones, D.; Jurrus, E.; Keller, T.; Matsumoto, S.; Mendoza, E.; Nordwall, D.; Olander, M.; Palmer, B.; Peden, N.; Schuchardt, K.; Stephan, E.; Taylor, H.; Thomas, G.; Vorpagel, E.; Windus, T. *Ecce, A Problem Solving Environment for Computational Chemistry, Software Version 1.5*; Pacific Northwest National Laboratory: Richland, WA 99352-0999, 2000.

(42) (a) Albright, T. A.; Burdett, J. K.; Whangbo, M. H. *Orbital Interactions in Chemistry*; Wiley: New York, 1985. (b) Hoggins, J. T.; Steinfink, H. *Inorg. Chem.* **1976**, *15*, 1682.

(43) (a) Flint, D. H.; Allen, R. M. *Chem. Rev.* **1996**, *96*, 2315. (b) Beinert, H. B.; Kennedy, M. C.; Strout, C. D. *Chem. Rev.* **1996**, *96*, 2335.

(44) Yang, X.; Wang, X. B.; Niu, S. Q.; Pickett, C. J.; Ichiye, T.; Wang, L. S. *Phy. Rev. Lett.* **2002**, *89*, 163401.